Path Continuity for Multi-Wheeled AGVs

Mirko Kokot, Damjan Miklić, and Tamara Petrović

***Abstract*—Notwithstanding the growing presence of AGVs in the industry, there is a lack of research about multi-wheeled AGVs which offer higher maneuverability and space efficiency. In this letter, we present generalized path continuity conditions as a continuation of previous research done for vehicles with more constrained kinematic capabilities. We propose a novel approach for analytically defining various kinematic modes (*motion modes*), that AGVs with multiple steer&drive wheels can utilize. This approach enables deriving vehicle kinematic equations based on the vehicle configuration and its constraints, path shape, and corresponding motion mode. Finally, we derive general continuity conditions for paths that multi-wheeled AGVs can follow, and show through examples how they can be utilized in layout design methods.**

***Index Terms*—Autonomous vehicle navigation, motion and path planning, kinematics, wheeled robots.**

I. Introduction

TODAY, the presence of automated guided vehicles (AGVs) in the industry is on a constant rise, especially in logistics and warehousing applications. This was spurred by the growing e-commerce sector and economy globalization, demanding an ever-increasing throughput of goods. Beyond closing the labor shortage gap, AGVs are also space efficient and represent valuable warehouse assets [1]. The majority of AGVs in the industry are based on Ackermann steering geometry, i.e., their kinematic models can be simplified to a bicycle model, or utilize differential drives. This simplifies the motion planning problem since kinematic constraints of such vehicles enable them to move only in "forwards" and "backwards" directions. Recently, a growing number of industrial AGVs has been using multiple individually actuated steering and driving wheels (S/D wheels)[1],[2]. Such vehicles are sometimes called "quad" vehicles [2]. However, because the name "quad" is already used in different contexts in the robotics community (e.g., quadrotor UAVs), we will use the term *multi-wheeled automated guided vehicle*, abbreviated as MW-AGV in the rest of the paper. The kinematics of such vehicles can be described by the generalized bicycle model [3], where the vehicle *heading* (direction of vehicle velocity) is decoupled from its *orientation* (relative angle between vehicle and world coordinate frames), enabling higher maneuverability and more efficient use of available space compared to the simpler kinematic configurations [4].

Accurate path following is the fundamental task of any AGV, and it is typically implemented as a sequence of several steps. The first step is *layout design*, where all permissible routes are laid out in advance, as a network of nodes and segments. During operation, a path planner *assigns routes* to vehicles, as sequences of segments to be followed, taking into consideration task allocation, conflict avoidance and system throughput. Once a route has been assigned, the onboard controller performs velocity planning, i.e., it calculates a nominal trajectory that includes velocity and steering references. Finally, an online controller calculates setpoint corrections based on current path tracking errors. To achieve path following accuracy and avoid dangerous oscillations, especially at high velocities, it is fundamental to ensure path continuity in the layout design step. For safety reasons, additional path continuity checks are often performed in the velocity planning phase.

Two common types of curve continuities are often considered in mathematics, namely, *geometric continuity* and *parametric continuity*. Whereas geometric continuity requires the geometric shape of curves to be continuous, parametric continuity also requires that the underlying parametrization be continuous as well [5]. Early methods for path planning acknowledged the problem of path continuity, but they usually opted for paths generated by stitching linear segments with circular arcs and cycloids for turning. Such paths were sufficiently smooth for rudimentary navigation algorithms, even though the generated paths are usually only 1st order geometrically continuous (G_1). Earliest research into path continuity [6] showed that such approach is not appropriate, and introduced paths based on the 2nd order geometric continuity (G_2), often called curvature continuity. Paths with G_2 continuity ensure not only vehicle orientation, but also wheel steering angle continuity. This approach is most widely utilized today, and there already exists a significant body of research regarding AGV motion planning based on G_2-paths with different optimization variants [7]–[9]. However, in [10] it was shown that that G_2-paths do not guarantee smooth and precise path tracking in the presence of additional steering constraints such as steering velocity limits. Instead, G_3-paths need to be utilized. It is important to note that AGV kinematic models in those articles are based on Ackermann steering geometry or utilize differential drives. To the best of our knowledge, very few papers [3], [4], [11], [12] address MW-AGVs, and none of them deal with the topic of path continuity for this kind of vehicle.

In papers which do address MW-AGVs, similar to the current industry standard, they acknowledge their versatile kinematic

Manuscript received March 1, 2021; accepted June 25, 2021. Date of publication July 26, 2021; date of current version August 3, 2021. This work was supported by (organizations/grants which supported the work). *(Corresponding author: Mirko Kokot.)*

Mirko Kokot and Damjan Miklić are with the Romb Technologies d.o.o., 10000 Zagreb, Croatia (e-mail: mirko.kokot@fer.hr; damjan@romb-technologies.hr).

Tamara Petrović is with the Department of Electrical Engineering and Computing, University of Zagreb, Zagreb 10000, Croatia (e-mail: tamara.petrovic@fer.hr).

Digital Object Identifier 10.1109/LRA.2021.3099086

[1]https://www.elettric80.com/en/products/laser-guided-vehicles/quad/

[2]https://www.systemlogistics.com/usa/news/news/shark

capabilities and observe them as distinct *kinematic modes*. Most often used kinematic modes include "tangential," "crab," and "differential" modes. This results in developing a separate specialized navigation approach for each kinematic mode with discrete transitions between them.

In this paper we are aiming to answer the following question: "What conditions does the path have to satisfy in order to guarantee smooth motion of MW-AGVs?". In answering this question, this paper makes the following contributions. First, we propose a unified and generalized approach to describing the versatile kinematic capabilities of MW-AGVs. We achieve this by defining *motion mode* as a function of vehicle orientation along the path and apply it to derive generalized vehicle kinematic equations. These equations can be used to calculate nominal steering and speed limit profiles which are inputs for several optimal velocity planning methods described in the literature, e.g., [13]–[16]. Our second contribution is a formal proof of path continuity conditions which build upon the proposed definition of motion modes and guarantee smooth motion of any AGV. We demonstrate how path continuity conditions can be used in layout design, and additionally we point out how they can be used as a simple validity check for existing paths (useful at both route assignment and velocity planning steps as a check if selected route is even feasible to traverse in a smooth manner).

In Section II we derive generalized vehicle kinematic equations based on the vehicle configuration and its path. In Section III we propose a way to define different motion modes which describe how the vehicle orientation changes along the path. Path continuity conditions are derived and explained in Section IV, and an example of how they can be applied in layout design and route assignment steps is shown in Section V.

II. Vehicle Kinematic Equations

We define the vehicle model as a set $V = \{w_1, w_2, \ldots, w_m\}$ with m actuated wheels w. Its configuration is defined by the position of each wheel in the vehicle-fixed frame of reference $\mathbf{r}_w, \forall w \in V$. By including the maximum traction speed v_w^{max} and maximum steering velocity ω_w^{max} of each wheel, we can describe a single wheel as a tuple $w = \langle < \mathbf{r}_w, v_w^{max}, \omega_w^{max} \rangle >$. This definition is sufficient for the scope of this article, but additional vehicle parameters could be added, e.g., maximum acceleration, time constants, wheel mounting angle, etc. In the rest of the document, expressions that are analogous for each wheel will be denoted with the use of subscript $w, \forall w \in V$.

Fig. 1 illustrates a MW-AGV with two S/D wheels. All of the values in this article are presented in the arbitrarily selected world-fixed frame of reference, unless explicitly stated otherwise. The vehicle-fixed frame of reference is centered on the vehicle tracking point, which can be an arbitrarily selected point within the vehicle footprint. Wheel-fixed frames are centered on the contact point of each wheel with the surface.

We define a *path* as a sequence of *segments* $P = \{P_1, P_2, \ldots\}$, where a single segment is defined as a tuple $P_k = \langle < \mathbf{C}_k(u), \theta_k(u), v_k^{max} \rangle >$. Parameter u is used for parametric representation of all equations in this document. A parametric curve $\mathbf{C}_k(u) = \begin{bmatrix} x(u) & y(u) \end{bmatrix}^T$ represents the nominal vehicle path, the function $\theta_k(u)$ describes the evolution of vehicle orientation along the path, and a vehicle speed limit v_k^{max} is assigned to each segment due to traffic or other safety reasons. In the rest of the document, expressions written in the form $f(u)$ imply $f_k(u), \forall P_k \in P$.

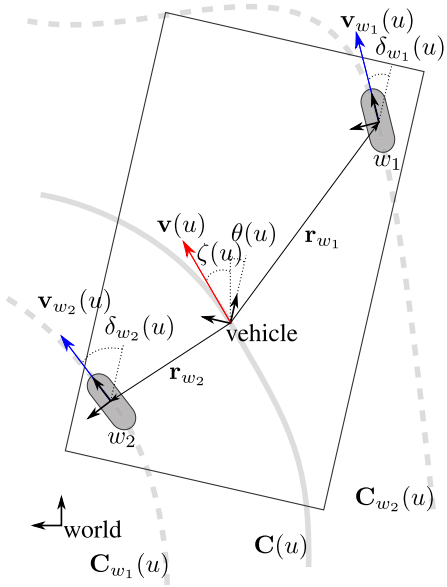

Fig. 1. An illustration of a MW-AGV with two actuated wheels.

It is important to note that the MW-AGV can have arbitrary orientation when moving, so the vehicle heading angle ζ is not the same as the vehicle orientation angle θ. Orientation is defined as a measure of the angle between vehicle-fixed and world-fixed frames of reference, whereas heading is the direction of the vehicle velocity $\mathbf{v}(u)$ and is directly defined by the path $\mathbf{C}(u)$ tangent:

$$\begin{aligned}\mathbf{v}(u) &= \frac{d\mathbf{C}(u)}{dt} = \frac{d\mathbf{C}(u)}{du}\frac{du}{ds}\frac{ds}{dt} \\ &= v(u)\frac{\mathbf{C}'(u)}{\|\mathbf{C}'(u)\|_2} = v(u)\widehat{\mathbf{C}'}(u) \end{aligned} \tag{1}$$

$$\zeta(u) = \arctan2(C'_y(u), C'_x(u)) \tag{2}$$

To clarify, $ds/du = \|\mathbf{C}'(u)\|_2$ follows from the standard definition for arc length of parametric curve:

$$s(u_1, u_2) = \int_{u_1}^{u_2} \sqrt{\left(\frac{dC_x(u)}{du}\right)^2 + \left(\frac{dC_y(u)}{du}\right)^2}\, du \tag{3}$$

Additionally, we use $ds/dt = v(u)$ instead of $v(t)$ for brevity sake, since for any velocity profile $v(t)$, there exists reparameterization $v(u(t))$.

As can can be seen by the equation for the vehicle velocity (1), vehicle kinematics are considered in conjunction with geometric properties of the path. Beside the shape of the curve $\mathbf{C}(u)$, the corresponding $\theta(u)$ is also an integral part for describing vehicle kinematics, e.g., vehicle angular velocity is determined as the rate of change of its orientation:

$$\omega(u) = \frac{d\theta(u)}{dt} = \frac{d\theta(u)}{du}\frac{du}{ds}\frac{ds}{dt} = v(u)\frac{\theta'(u)}{\|\mathbf{C}'(u)\|_2} \tag{4}$$

In the scope of this paper, we only look at S/D wheels whose steering axis passes through its contact point with the surface, i.e., without steering offset [3]. If the vehicle is moving along parametric path $\mathbf{C}(u)$ with orientation $\theta(u)$, the path each individual wheel w will traverse can be defined by the parametric function:

$$\mathbf{C}_w(u) = \mathbf{C}(u) + \mathbf{R}(\theta(u))\mathbf{r}_w, \tag{5}$$

where $\mathbf{R}(\theta)$ is the standard two dimensional rotation matrix.

From (5), wheel traction velocity $\mathbf{v}_w(u)$ can be calculated analogously to (1):

$$\mathbf{v}_w(u) = \frac{d\mathbf{C}_w(u)}{dt} = \frac{d\mathbf{C}_w(u)}{du}\frac{du}{ds}\frac{ds}{dt} = v(u)\frac{\mathbf{C}'_w(u)}{\|\mathbf{C}'(u)\|_2} \tag{6}$$

The heading of each wheel can also be calculated analogously to (2), and it is important to note that wheel heading and its orientation are always equal or opposite, i.e., 180° apart, when wheel traction speed is negative. In this article we treat speed as measure of velocity which means that it is always positive, but care must be taken in the implementation in case of reversing. With $v_w(u) > 0$, the steering angle depends on current wheel heading and vehicle orientation, hence the steering angle $\delta_w(u)$ and steering velocity $\omega_w(u)$ of each wheel are calculated by the following equations:

$$\delta_w(u) = \zeta_w(u) - \theta(u) \tag{7}$$

$$\omega_w(u) = \frac{d\delta_w(u)}{dt} = \frac{d\zeta_w(u)}{dt} - \frac{d\theta(u)}{dt} = \kappa_w(u)v_w(u) - \omega(u) \tag{8}$$

Curvature $\kappa(u)$ of some planar curve $\mathbf{C}(u)$ is given by the following well-known equation:

$$\kappa(u) = \frac{\mathbf{C}'_x(u)\mathbf{C}''_y(u) - \mathbf{C}''_x(u)\mathbf{C}'_y(u)}{\left(\mathbf{C}'_x{}^2(u) + \mathbf{C}'_y{}^2(u)\right)^{\frac{3}{2}}} = \frac{\det(\mathbf{C}'(u), \mathbf{C}''(u))}{\|\mathbf{C}'(u)\|_2^3} \tag{9}$$

Vehicle speed limit is defined as the fastest speed $v^{max}(u)$ that allows ideal following of the path P_k while adhering to the constraints, i.e., segment speed limit v_k^{max}, maximum traction speed v_w^{max}, and maximum steering velocity ω_w^{max}. For straight segments, and those with small curvature, typically the only limiting factors are segment speed limit v_k^{max} and maximum traction speed v_w^{max}, but in cases where the vehicle is making turns on paths with pronounced curvature, it may need to slow down so that steering actuators can keep up, i.e., making sure that maximum steering velocity ω_w^{max} is sufficient so that the vehicle does not veer of the path. From equations (6) and (8), it can be seen that the shape of the path $\mathbf{C}(u)$ and vehicle orientation $\theta(u)$ explicitly tie vehicle speed $v(u)$ to wheel traction speed $v_w(u)$ and steering velocity $\omega_w(u)$. We introduce the symbols R_w^v and R_w^ω to denote these ratios:

$$R_w^v(u) = \frac{v_w(u)}{v(u)} = \frac{\|\mathbf{v}_w(u)\|_2}{\|\mathbf{v}(u)\|_2} = \frac{\|\mathbf{C}'_w(u)\|_2}{\|\mathbf{C}'(u)\|_2} \tag{10}$$

$$R_w^\omega(u) = \frac{\omega_w(u)}{v(u)} = \frac{\kappa_w(u)\,\|\mathbf{C}'_w(u)\|_2 - \theta'(u)}{\|\mathbf{C}'(u)\|_2} \tag{11}$$

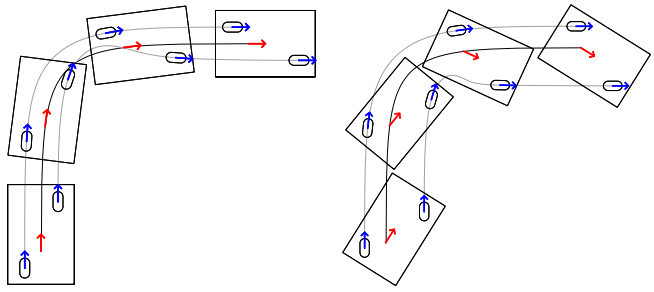

(a) $\alpha = 0^\circ$ (b) $\alpha = -32^\circ$

Fig. 2. Examples of "tangential" mode with different values for the angle offset α. Colored arrows represent orientation.

Given the maximum traction speed v_w^{max} and maximum steering velocity ω_w^{max} of each actuated wheel combined with (10), (11), and segment speed limit v_k^{max}, we can express the vehicle speed limit as:

$$v^{max}(u) = \min\left(v_k^{max}, \min_{w\in V}\frac{v_w^{max}}{R_w^v(u)}, \min_{w\in V}\frac{\omega_w^{max}}{R_w^\omega(u)}\right) \tag{12}$$

Additionally, by combining (12) with (10), the traction speed limit of each individual wheel can be defined as $v_w^{max}(u) = v^{max}(u)R_w^v(u)$. This can be used as an input for several optimal velocity planning methods described in the literature, e.g., [13]–[16].

III. Motion Modes

In the previous section, one can notice that the vehicle orientation function $\theta(u)$ can be specified arbitrarily during path segment definition. In practice, path segments for MW-AGVs usually come with assigned corresponding *kinematic modes* that the vehicle must use and in this section we demonstrate how they can be defined in a unified manner as vehicle orientation function $\theta(u)$. Examples of commonly used MW-AGV kinematic modes are "tangential" where vehicle orientation is same or opposite to its heading $\zeta(u)$, "crab" where the orientation is constant, and "differential" where the change of orientation is achieved by applying different velocity setpoints to the wheels, without changing their steering angles [4], [11], [12]. In this paper, we propose a broader definition of a kinematic mode, called *motion mode*, which can encapsulate multiple kinematic modes under a single expression.

A *motion mode* is a function of u that defines the evolution of vehicle orientation along its path $\mathbf{C}(u)$. Using this definition, we can capture different ways in which a vehicle is driving along its path, including traditional kinematic modes, but also arbitrary non-standard driving behaviours.

For "tangential" mode, we propose a broader definition which allows for an arbitrary angle offset α between vehicle heading and orientation (Fig. 2):

$$\theta_{tangential}(u) = \zeta(u) + \alpha \tag{13}$$

In the case of vehicles using Ackermann steering geometry or differential drive vehicles, their kinematic constraints only

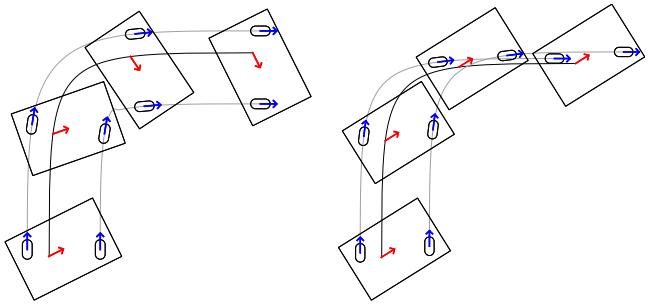

(a) "Tangential" mode with angle offset $\alpha = -63.44°$, i.e., "differential" mode

(b) "Crab" mode with angle offset $\alpha = -32°$

Fig. 3. Examples of an MW-AGV using "differential" and "crab" modes.

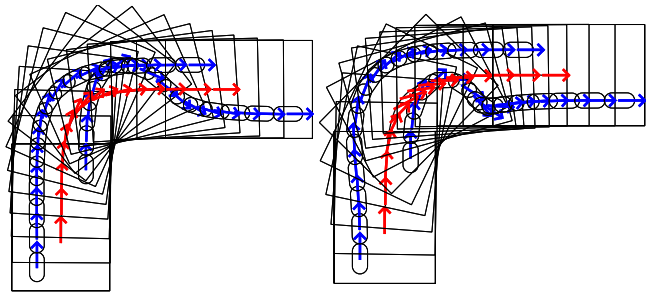

Fig. 4. Comparison of vehicle footprint along the path between "tangential" mode (left) and "exponential" mode (right) with $n = 1.7$ applied to (17). Both motion modes use angle offset $\alpha = 0°$.

allow them to drive in "tangential" mode with the angle offset $\alpha = 0°$ (Fig. 2(a)) and $\alpha = 180°$, i.e., they can move only in "forwards" and "backwards" direction. Also, for MW-AGVs whose wheels and tracking point are collinear, "differential" mode can be defined as special case of (13), achieved by:

$$\alpha = \arctan \frac{r_{w_1 x} - r_{w_2 x}}{r_{w_2 y} - r_{w_1 y}} \tag{14}$$

The resulting heading is always perpendicular to the line connecting S/D wheels and as a result, wheels do not change their steering angle (Fig. 3(a)). With this, we can see that equations presented in Section II can also be applied to vehicles with simpler kinematic configurations by choosing the appropriate motion mode.

The third commonly used motion mode is "crab" mode (Fig. 3(b)):

$$\theta_{crab}(u) = \alpha \tag{15}$$

An example of a non-standard motion mode we found useful in practice is the "exponential" mode. With it, one can change the timing of the turning maneuver so that it is easier to enter/exit narrow aisles or to make turns near a wall. Depending on the use case, two definitions are presented. A delayed turning maneuver has the following reparameterization:

$$\theta_{exp}(u) = \zeta(u^n) + \alpha, n > 1 \tag{16}$$

whereas an anticipated turning maneuver is achieved by a symmetrical reparameterization:

$$\theta_{exp}(u) = \zeta(1 - (1-u)^n) + \alpha, n > 1 \tag{17}$$

In both cases, the value for n is determined depending on the shape of the curve $\mathbf{C}(u)$ and the surroundings. With (16) and (17), by influencing the timing of the turning maneuver, the vehicle footprint along the path can also be reduced as shown in Fig. 4.

IV. Path Continuity

As it was shown in previous works [6]–[10], path continuity is crucial to ensure smooth and error-free motion for any real vehicle with finite actuator speed. So far, path continuity constraints have been analyzed only for vehicles with simpler kinematic models, where G_3-paths have been proven sufficient. In this paper, we expand on previous research and provide generalized path continuity constraints that also include MW-AGVs driven by continuous linear and angular velocity commands for each actuated wheel, such that no slippage occurs. By taking advantage of (10) and (11), we can simplify this as observing the motion of an AGV with some continuous speed $v(u)$ along curve $\mathbf{C}(u)$ utilizing motion mode $\theta(u)$.

A curve $\mathbf{C}(u)$ is considered to have nth order geometric continuity (G_n) for some value of parameter u if and only if there exists a set of shape parameters $\{\beta_1, \beta_2, \ldots, \beta_n\}$ with $\beta_1 > 0$ for which the following conditions are true [5]:

$$\mathbf{C}(u^-) = \mathbf{C}(u^+) \tag{18}$$

$$\mathbf{C}'(u^-) = \beta_1 \mathbf{C}'(u^+) \tag{19}$$

$$\mathbf{C}''(u^-) = \beta_1^2 \mathbf{C}''(u^+) + \beta_2 \mathbf{C}'(u^+) \tag{20}$$

$$\mathbf{C}'''(u^-) = \beta_1^3 \mathbf{C}'''(u^+) + 2\beta_1\beta_2 \mathbf{C}''(u^+) + \beta_3 \mathbf{C}'(u^+)$$

$$\cdots \tag{21}$$

$$\mathbf{C}^{(n)}(u^-) = \beta_1^n \mathbf{C}^{(n)}(u^+) + \cdots + \beta_n \mathbf{C}'(u^+) \tag{22}$$

where $f(u^{\pm})$ implies the limit $lim_{x \to u^{\pm}} f(x)$.

Parametric continuity is a special case where the $\beta_1 = 1$ and $\beta_i = 0, \forall i \in [2, n]$, i.e., first n curve derivatives are equal, and is usually denoted as C_n.

Definition 1: By smooth motion, we consider at least G_0 continuity of position and orientation of both the vehicle and its wheels, their linear and angular velocities, vehicle heading $\zeta(u)$ and its rate of change.

To provide the necessary context for stating the theorem, we note that first two derivatives of wheel path (5) are given by:

$$\mathbf{C}'_w(u) = \mathbf{C}'(u) + \theta'(u)\mathbf{R}'(\theta(u))\mathbf{r}_w \tag{23}$$

$$\mathbf{C}''_w(u) = \mathbf{C}''(u) + \theta''(u)\mathbf{R}'(\theta(u))\mathbf{r}_w + \theta'^2(u)\mathbf{R}''(\theta(u))\mathbf{r}_w \tag{24}$$

From (23), it can be seen that if $\mathbf{C}'(u)$ and $\mathbf{R}'(\theta(u))\mathbf{r}_w$ are linearly dependent, vehicle velocity (1) and wheel velocity (6) are parallel vectors.

Theorem 1: Any path driven by an AGV, with some continuous speed $v(u^-) = v(u^+)$ and $v(u) \neq 0$, such that $\mathbf{C}'(u)$

and $\mathbf{R}'(\theta(u))\mathbf{r}_w$ are linearly independent for at least one wheel w, results in smooth motion if and only if its curve $\mathbf{C}(u)$ and motion mode $\theta(u)$ are at least G_2 continuous with identical shape parameters $\{\beta_1, \beta_2\}$.

This theorem imposes a key requirement on the layout design step of AGV control. It requires paths consisting of multiple segments to be designed in such a manner that the curves of consequent segments and their motion modes are G_2 continuous at cross-over points.

Proof. Continuity of vehicle position is by definition equivalent to G_0 curve continuity:

$$\mathbf{C}(u^-) = \mathbf{C}(u^+) \tag{25}$$

Analogously, continuity of vehicle orientation is by definition equivalent to G_0 motion mode continuity:

$$\theta(u^-) = \theta(u^+) \tag{26}$$

From (2), continuity of vehicle heading $\zeta(u^-) = \zeta(u^+)$ is guaranteed if and only if the path is at least G_1 continuous:

$$\mathbf{C}'(u^-) = \beta_1 \mathbf{C}'(u^+), \beta_1 \in \mathbb{R}^+ \tag{27}$$

Expanding the continuity of vehicle angular velocity $\omega(u^-) = \omega(u^+)$ as (4) and substituting (27) directly shows equivalence to the motion mode G_1 continuity:

$$\theta'(u^-) = \beta_1 \theta'(u^+) \tag{28}$$

The rate of change of vehicle heading $\dot{\zeta}(u)$ is defined as:

$$\dot{\zeta}(u) = \frac{d\zeta(u)}{dt} = \frac{d\zeta(u)}{ds}\frac{ds}{dt} = \kappa(u)v(u) \tag{29}$$

From (29) it follows that the rate of change of vehicle heading is continuous, i.e., $\dot{\zeta}(u^-) = \dot{\zeta}(u^+)$, given continuous linear velocity v(u), if and only if the path has curvature continuity $\kappa(u^-) = \kappa(u^+)$ (G_2 continuity), i.e., the following expression is also true [5]:

$$\mathbf{C}''(u^-) = \beta_1^2 \mathbf{C}''(u^+) + \beta_2 \mathbf{C}'(u^+), \beta_2 \in \mathbb{R} \tag{30}$$

Since wheel orientation and heading are always equal or opposite (when $v_w(u) < 0$), an approach analogous to vehicle heading is applied to the continuity of wheel orientation:

$$\mathbf{C}'_w(u^-) = \beta_{w1} \mathbf{C}'_w(u^+), \beta_{w1} \in \mathbb{R}^+ \tag{31}$$

Expanding (31) with (5) and substituting (27) and (28) yields $\beta_1 = \beta_{w_1}$. With this the continuity of wheel traction speed $v_w(u^-) = v_w(u^+)$ is already guaranteed by expanding (6).

Lastly, by expanding wheel steering velocity continuity $\omega_w(u^-) = \omega_w(u^+)$ with (8) and substituting (4), (27) and (28), it can be simplified as $\kappa_w(u^-) = \kappa_w(u^+)$, i.e., it is continuous if and only if the path that each wheel traverses is G_2 continuous:

$$\mathbf{C}''_w(u^-) = \beta_{w1}^2 \mathbf{C}''_w(u^+) + \beta_{w2} \mathbf{C}'_w(u^+), \beta_{w2} \in \mathbb{R} \tag{32}$$

By substituting (23), (24), (27), (28), and (30) into (32), it can be reordered as:

$$\begin{aligned}&(\beta_2 - \beta_{w_2})\,\mathbf{C}'(u^+) + \\ &\left(\theta''(u^-) - \beta_1^2\theta''(u^+) - \beta_{w2}\theta'(u^+)\right)\mathbf{R}'(\theta(u^+))\mathbf{r}_w = 0\end{aligned} \tag{33}$$

From (33), linear independence of $\mathbf{C}'(u)$ and $\mathbf{R}'(\theta(u))\mathbf{r}_w$ directly shows that $\beta_2 = \beta_{w_2}$ and motion mode G_2 continuity are sufficient and necessary:

$$\theta''(u^-) = \beta_1^2\theta''(u^+) + \beta_2\theta'(u^+) \tag{34}$$

□

Corollary 1: Any path driven by the AGV, with some continuous speed $v(u^-) = v(u^+)$ and $v(u) \neq 0$, such that $\mathbf{C}'(u)$ and $\mathbf{R}'(\theta(u))\mathbf{r}_w$ are linearly dependent for all wheels w, results in smooth motion if and only if its curve $\mathbf{C}(u)$ is at least G_2 continuous and its motion mode $\theta(u)$ is at least G_1 continuous with identical shape parameter β_1.

Proof. Expanded continuity of curvature of wheel path $\kappa_w(u^-) = \kappa_w(u^+)$ with (9):

$$\frac{\det(\mathbf{C}'_w(u^-), \mathbf{C}''_w(u^-))}{\|\mathbf{C}'_w(u^-)\|_2^3} = \frac{\det(\mathbf{C}'_w(u^+), \mathbf{C}''_w(u^+))}{\|\mathbf{C}'_w(u^+)\|_2^3} \tag{35}$$

This can be reordered by substituting (31):

$$\det\left(\mathbf{C}'_w(u^+), \mathbf{C}''_w(u^-) - \beta_1^2\mathbf{C}''_w(u^+)\right) = 0 \tag{36}$$

By substituting (23) and (24) into (36) we get the final expression:

$$\begin{aligned}&\det\left(\mathbf{C}'(u^+) + \theta'(u^+)\mathbf{R}'(\theta(u^+))\mathbf{r}_w,\right. \\ &\left.\beta_2\mathbf{C}'(u^+) + \left(\theta''_1(u^+) - \beta_1^2\theta''_2(u^+)\right)\mathbf{R}'(\theta(u^+))\mathbf{r}_w\right) = 0\end{aligned} \tag{37}$$

From this, curvature continuity of wheel path is guaranteed by linear dependence of $\mathbf{C}'(u^+)$ and $\mathbf{R}'(\theta(u^+))\mathbf{r}_w$, hence motion mode G_1 continuity is sufficient and necessary. □

An example when the corollary is applicable are "differential" mode where all the wheels have constant steering angle and are collinear with each other and with the vehicle tracking point. Another example is "crab" mode where vehicle orientation is constant. It is also convenient to note that in the case when the vehicle is standing still at some point on its path, i.e., $v(u) = 0$, continuity conditions for both rate of change of vehicle heading and wheel angular velocity are satisfied by default. This means that for the vehicle to resume its motion from this point, it is sufficient that the curve $\mathbf{C}(u)$ and its corresponding motion mode $\theta(u)$ are G_1 continuous. An example of where this could be useful are points on the path where the vehicle reverses its heading.

The stated continuity constraints must be taken into account in the layout design phase, when connecting segments. They should also be checked at the vehicle controller level, to verify path validity in the velocity planning phase. This can be easily done by determining $\{\beta_1, \beta_2\}$ from (28) and (34), and then checking G_2 continuity of corresponding curves by applying them to (27) and (30).

V. Application Examples

In this section we will demonstrate how path continuity constraints can be used in layout design. In the first example we examine a MW-AGV with two actuated wheels traversing two segments in "tangential" mode where path continuity conditions are not satisfied. Conversely, in the second example we

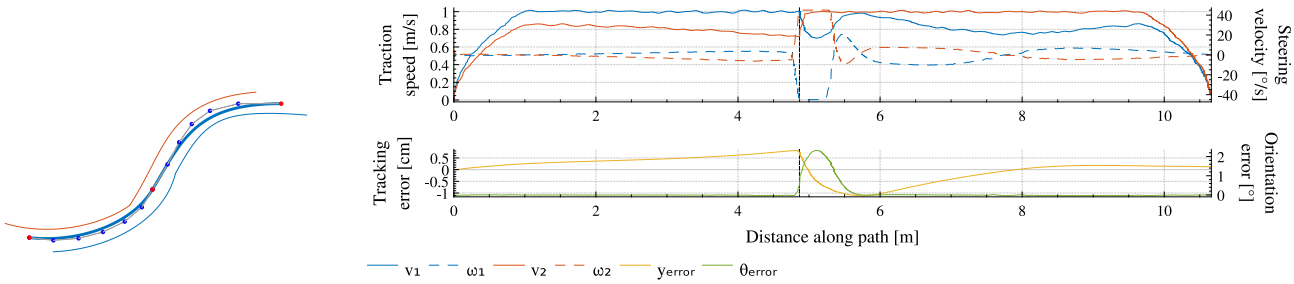

(a) Nominal paths for vehicle and its two actuated wheels $w1$ (blue) and $w2$ (red) in the example V-A. Blue and red dots represent Bézier control points.

(b) In the top graph it can be seen that steering velocities of both wheels reach their maximum values after the segment junction, followed by steering oscillations. The tracking error (lateral distance of the vehicle tracking point from the nominal path) grows to $\approx 1.25\text{cm}$, while the orientation error maximum reaches $\approx 2.5^\circ$.

Fig. 5. Simulation of MW-AGV motion with MPC path following controller. Both path segments utilize "tangential" mode with $\alpha = 0^\circ$ and their parametric curves are G_1 continuous.

TABLE I
CONTROL POINTS FOR BÉZIER CURVES USED IN EXAMPLES

	Example V-A	Example V-B	Example V-C
$\mathbf{C}_1(u)$	(0.188, 3.187)	(0.188, 3.187)	(0.188, 3.187)
	(1.031, 3.281)	(1.031, 3.281)	(1.031, 3.281)
	(1.913, 3.212)	(1.913, 3.212)	(1.913, 3.212)
	(2.766, 2.991)	(2.766, 2.991)	(2.766, 2.991)
	(3.525, 2.625)	(3.525, 2.625)	(3.750, 2.750)
	(4.125, 2.125)	(4.125, 2.125)	(3.937, 2.437)
	(4.500, 1.500)	(4.500, 1.500)	(4.500, 1.500)
$\mathbf{C}_2(u)$	(4.500, 1.500)	(4.500, 1.500)	(4.500, 1.500)
	(5.025, 0.625)	(4.823, 0.962)	(4.725, 1.125)
	(5.430, 0.150)	(5.026, 0.253)	(5.137, 0.437)
	(5.873, 0.787)	(5.032, 0.765)	(5.873, 0.787)
	(6.510, 1.250)	(6.510, 1.250)	(6.510, 1.250)
	(7.500, 1.500)	(7.500, 1.500)	(7.500, 1.500)
	(9.000, 1.500)	(9.000, 1.500)	(9.000, 1.500)

demonstrate how to achieve path continuity for these segments and examine its effects on vehicle motion. Finally, in the third example we demonstrate how to achieve path continuity for segments with "differential" and "crab" mode.

We are considering a MW-AGV model with two actuated wheels. Wheels are positioned on the diagonal of the vehicle with $\mathbf{r}_{w1} = [0.89, -0.40]$ m and $\mathbf{r}_{w2} = [-0.89, 0.40]$ m. In the figures, they are represented with blue and red colors respectively. For the purpose of providing simulation examples, we have set the maximum traction speed to $v_w^{max} = 1$ m/s and maximum steering velocity to $\omega_w^{max} = 45\ ^\circ/\text{s}$, which roughly correspond to commercially available AGV steering and traction drives. The simulations were performed in Simulink using a kinematic vehicle model with first order lag on steering and traction. A Model predictive controller (MPC) is used for path following, which represents the current state-of-the art in AGV navigation. Path segments are given as 6th order Bézier curves with start and end control points colored red in the figures.

A. *Failure to Satisfy the Continuity Conditions*

The Bézier curves in this example are only G_1 continuous with control points given in Table I, column V-A. They represent the *initial path* that will be optimized in the following examples. Fig. 5(a), shows exact nominal paths for the vehicle-fixed frame and both wheels. To the human eye this path might look smooth. In the Fig. 5(b) traction and steering velocities of both wheels resulting from simulated motion of MW-AGW along the path are presented. In the top graph, steering velocities of both wheels reach their maximum values, hence vehicle is unable to track path accurately. As a result, both tracking and orientation error grow and steering inputs enter into oscillatory behaviour to compensate.

B. *Motion Mode and Curve Continuity for Tangential Motion*

Now we examine how path continuity constraints can be applied to segments using "tangential" mode with $\alpha = 0^\circ$. First, we will show that in case of "tangential" mode, motion mode G_2 continuity is equivalent to path G_3 continuity which ensures that $d\kappa(u)/ds$ is continuous, i.e., $\kappa'(u^-) = \beta_1 \kappa'(u^+)$. From (13) we can see that $\omega(u) = \dot{\zeta}(u)$, and combining this with (4) and (29) we can get following expressions for $\kappa(u)$ and its derivative:

$$\kappa(u) = \frac{\theta'(u)}{\|\mathbf{C}'(u)\|_2} \tag{38}$$

$$\kappa'(u) = \frac{\theta''(u)}{\|\mathbf{C}'(u)\|_2} - \theta'(u)\frac{\mathbf{C}'(u)\cdot\mathbf{C}''(u)}{\|\mathbf{C}'(u)\|_2^3} \tag{39}$$

From (38) it is trivial to show that path G_2 continuity $\kappa(u^-) = \kappa(u^+)$ implies (28) by combining it with (27). Similarly, from (39) we can show that path G_3 continuity $\kappa'(u^-) = \beta_1\kappa'(u^+)$ implies (34) by combining it with (27), (28), and (30).

To ensure path continuity for segments from the first example, it is sufficient to select some shape parameters $\{\beta_1, \beta_2, \beta_3\}$ for G_3 continuity and modify the curves accordingly. Since this problem is underdetermined, we have selected shape parameters that yield minimal travel time for $\mathbf{C}_2(u)$. The resulting control points are provided in Table I, column V-B. In Fig. 6(a), we can

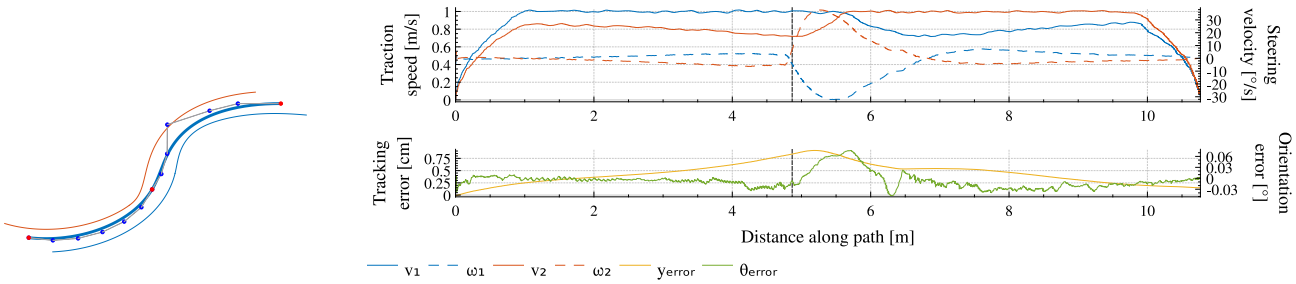

(a) Nominal paths for vehicle and its two actuated wheels $w1$ (blue) and $w2$ (red) in the example V-B.

(b) In the top graph it can be seen that steering velocities of both wheels have smooth responses without oscillations. The maximum tracking error is $\approx 0.5\text{cm}$, while the orientation error is commeasurable with noise $\approx 0.075°$.

Fig. 6. Simulation of MW-AGV motion with MPC path following controller. Both path segments utilize "tangential" mode with $\alpha = 0°$ and their parametric curves are G_3 continuous.

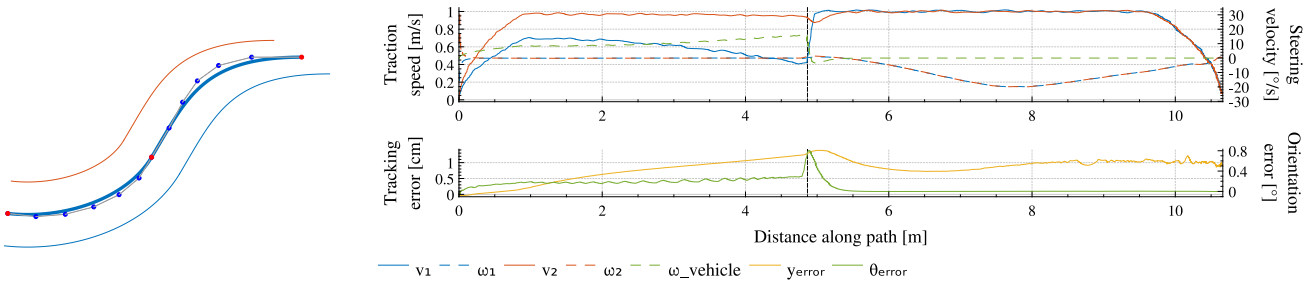

(a) Initial nominal paths for vehicle and its two actuated wheels $w1$ (blue) and $w2$ (red) in the example V-C.

(b) In the top graph, vehicle angular velocity has a sudden change followed by overshoot at segment junction resulting in an orientation error peak $\approx 0.8°$.

Fig. 7. Simulation of MW-AGV motion with MPC path following controller. First segment is driven in "differential" mode with $\alpha = -65.8°$ and second segment in "crab" mode $\alpha = -6.76°$. Path is G_1 continuous at segment junction.

see that the nominal paths retained similar shape to the original example, but by comparing Fig. 5(b) and Fig. 6(b), we can see different MW-AGV behaviour. As a result of path G_3 continuity, we can observe smooth and controlled change in steering velocities of both wheels, without subsequent oscillations. Even more importantly, both tracking and orientation errors are significantly reduced.

C. Motion Mode and Curve Continuity From "differential" to "crab" Mode

In the final example, we look at a motion modes transition along the same path. Along the first segment, the vehicle drives in "differential" mode ("tangential" with $\alpha = -65.8°$). Along the second segment, the vehicle drives in "crab" mode with $\alpha = -6.76°$, keeping the orientation attained at the end of the first segment.

In Fig. 7(a) we can see that wheel paths are continuous, since the path is G_1 continuous and vehicle and wheel velocities are always parallel vectors in both motion modes. A sudden change of vehicle angular velocity at the segment junction is clearly visible in Fig. 7(b). This causes an orientation error which is about twice as big as for the continuous segment junction. As our kinematic simulation model does not include vehicle inertia, we expect that this effect would be even more severe on a real vehicle.

In Fig. 8(a), the path is modified so that three control points from each curve are collinear at the segment junction (Table I, column V-C). This means that their second derivatives are zero at the junction point, i.e., paths are trivially G_2 continuous. This is needed so that "differential" mode is G_1 continuous with "crab" mode where orientation is constant, hence vehicle angular velocity at the junction must be zero for both segments. This satisfies Corollary 1. The result can be seen in Fig. 8(b) where vehicle angular velocity is reduced gradually before switching to "crab" mode.

The examples have been implemented using *dlib*[3] and *Bezier*[4] C++ libraries for optimization and parametric curve implementation. The application code used to generate the examples has been made available as open-source.[5]

[3]http://dlib.net/
[4]https://github.com/romb-technologies/Bezier
[5]https://github.com/romb-technologies/path_continuity

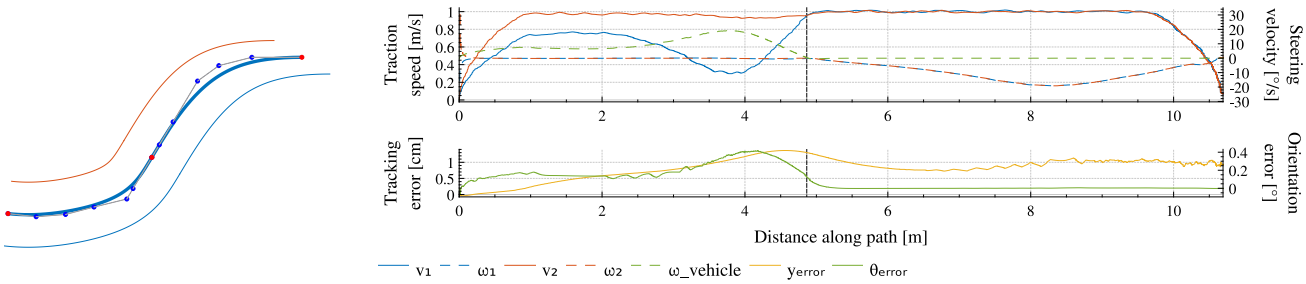

(a) Adjusted nominal paths for vehicle and its two actuated wheels $w1$ (blue) and $w2$ (red) in the example V-C.

(b) In the top graph it can be seen that vehicle angular velocity has smooth response without oscillations and the orientation error maximum is $\approx 0.4^\circ$.

Fig. 8. Simulation of MW-AGV motion with MPC path following controller. First segment is driven in "differential" mode with $\alpha = -65.8^\circ$ and second segment in "crab" mode $\alpha = -6.76^\circ$. Path is G_2 continuous at segment junction with $\mathbf{C}''(u) = \vec{0}$ for both segments.

VI. Conclusion

Previous research into path continuity of mobile robots dealt only with the most common kinematic configurations, such as bicycle and differential drive. On the other hand, existing research into MW-AGV kinematics observed its versatile maneuverability in context of separate kinematic modes. In this article our goal has been to generalize existing findings and to extend path continuity conditions to include MW-AGVs. We have defined generalized vehicle kinematic equations based on the shape of the path and corresponding motion mode. This kinematic formulation can be used to calculate nominal steering and speed limit profiles for trajectory planning. We have also proposed an unified approach for defining various *motion modes* as vehicle orientation function $\theta(u)$. Furthermore, we have derived generalized continuity rules, which represent necessary and sufficient conditions for smooth AGV motion. They can be used as a simple way to check the validity of existing paths or, as demonstrated by the presented examples, they can be used in layout design.

Our ongoing work is focused on developing navigation algorithms which apply the described generalized approach to path continuity.

References

[1] L. Harrington and R. Smith, "The supply chain talent shortage: from gap to crisis," Jul. 2017. [Online]. Available: https://www.dhl.com/global-en/home/press/press-archive/2017/the-impact-of-digitalization-and-status-of-the-supply-chain-profession-are-driving-a-global-talent-shortage-crisis.html

[2] "Automated guided vehicle (agv) drive configurations by type," *SCOTT*, Dec. 2019. [Online]. Available: https://www.scottautomation.com/news/articles/automated-guided-vehicle-agv-drive-configurations-by-type/

[3] A. Kelly, "A vector algebra formulation of kinematics of wheeled mobile robots," in *Proc. Int. Conf. Field Service Robot.*, 2010, pp. 1–14.

[4] V. Dave *et al.*, "Tuning procedure for correction of systematic errors in a quad configuration agv," in *Machines, Mechanism and Robotics*. Singapore: Springer, 2019, pp. 507–516.

[5] B. A. Barsky and A. D. DeRose, "Geometric continuity of parametric curves," EECS Department, University of California, Berkeley, Tech. Rep. UCB/CSD-84-205, Oct 1984. [Online]. Available: http://www2.eecs.berkeley.edu/Pubs/TechRpts/1984/5752.html

[6] W. Nelson, "Continuous-curvature paths for autonomous vehicles," in *Proc. IEEE Int. Conf. Robot. Automat.*, 1989, pp. 1260–1264.

[7] A. Scheuer and T. Fraichard, "Continuous-curvature path planning for car-like vehicles," in *Proc. IEEE/RSJ Int. Conf Intell. Robot Syst. Innov. Robot. Real-World Appl. IROS'97*, 1997, vol. 2, pp. 997–1003.

[8] F. Gómez-Bravo, F. Cuesta, A. Ollero, and A. Viguria, "Continuous curvature path generation based on β-spline curves for parking manoeuvres," *Robot. Auton. Syst.*, vol. 56, no. 4, pp. 360–372, 2008.

[9] A. M. Lekkas, A. R. Dahl, M. Breivik, and T. I. Fossen, "Continuous-curvature path generation using fermat's spiral," *Model., Identification Control*, vol. 34, no. 4, pp. 183–198, 2013.

[10] C. G. L. Bianco, A. Piazzi, and M. Romano, "Smooth motion generation for unicycle mobile robots via dynamic path inversion," *IEEE Trans. Robot.*, vol. 20, no. 5, pp. 884–891, Oct. 2004.

[11] R. Sakrikar *et al.*, "A material transfer system using automated guided vehicles," *Division of Remote Handling & Robotics, Technol. Develop. Article, BARC Newsletter*, no. 319, Mar.–Apr. 2011.

[12] D. Rosendahl, "Improvement of a measurement system for reflectors that are used for navigation of mobile units," M.S. Thesis, Luleå University of Technology, Jun. 2005, [Online]. Available: http://www.diva-portal.org/smash/get/diva2:1019696/FULLTEXT01.pdf.

[13] M. Raineri, S. Perri, and C. G. L. Bianco, "Online velocity planner for laser guided vehicles subject to safety constraints," in *Proc. IEEE/RSJ Int. Conf. Intell. Robots Syst.*, 2017, pp. 6178–6184.

[14] M. Raineri and C. G. L. Bianco, "Jerk limited planner for real-time applications requiring variable velocity bounds," in *Proc. IEEE 15th Int. Conf. Automat. Sci. Eng.*, 2019, pp. 1611–1617.

[15] V. Munoz, A. Ollero, M. Prado, and A. Simon, "Mobile robot trajectory planning with dynamic and kinematic constraints," in *Proc. IEEE Int. Conf. Robot. Automat.*, 1994, pp. 2802–2807.

[16] M. Brezak and I. Petrović, "Time-optimal trajectory planning along predefined path for mobile robots with velocity and acceleration constraints," in *Proc. IEEE/ASME Int. Conf. Adv. Intell. Mechatronics*, 2011, pp. 942–947.